Quantitative Potentials of Dynamic Emission Computed Tomography

Thomas F. Budinger, Stephen E. Derenzo, William L. Greenberg, Grant T. Gullberg, and Ronald H. Huesman

University of California, Berkeley, California

Statistical uncertainties in emission computed tomography were simulated in 60 computer studies involving various numbers of events and distributions of activity. Previous studies have shown that for a uniform disc of activity the rms percentage of uncertainty per resolution cell is: 120 × (number of resolution cells)$^{1/4}$ × (number of events per resolution cell)$^{-1/2}$.

In this work we examined the more general situation where one or two regions of uniform activity are surrounded by a uniform background, and found that for an equal number of recorded events the uncertainties were reduced when the activity was concentrated in a portion of the field. The empirical relation

$$\text{rms \% uncertainty in } n_t = 120(N)^{1/4}(n_t)^{-3/4},$$

where n_t is the number of events in an average target (organ) resolution cell and N is the total number of events recorded, satisfactorily described the relationships between uncertainties, contrast, total number of detected events, and number of resolution cells for all 60 computer studies.

By means of this relation, we show the theoretical possibility of gated cardiac imaging with 20% uncertainty in 1 cm × 1 cm regions, and of 1-sec cerebral blood-flow images with 20% uncertainty in 2 cm × 2 cm regions.

J Nucl Med 19: 309–315, 1978

One of the important potentials of emission computed tomography in nuclear medicine is the noninvasive quantitation of regional metabolic activity within the human body. Such quantitation is limited in most cases by the random uncertainties in the reconstructed images and these uncertainties are far greater than those expected from simple considerations of the number of events recorded from each resolution cell. For example, if the average number of reconstructed events is 400 per resolution cell, one might expect the rms uncertainty to be 5%. Actually, however, the rms uncertainty is about 44% for a circular region of uniform activity 62 resolution cells across, as calculated in Fig. 1.

The equation in Fig. 1 was developed in Ref. *1* from previous work (*2–7*) and is plotted in Fig. 2. Note that the pixel size is assumed to be as large as, or larger than, the resolution of the imaging system. The value 120 in Fig. 1 is appropriate in the absence of attenuation for the iterative reconstruction algorithms if the pixels are 1.5 times larger than the projection bins. For the convolution algorithms the equation in Fig. 1 also holds, but the value of 120 may be altered by the convolution kernel used.

In order to achieve 20% uncertainty in an image of 3,000 resolution cells we need 6 million events

Received July 18, 1977; revision accepted Nov. 9, 1977.

For reprints contact: Thomas F. Budinger, Donner Laboratory, University of California, Berkeley, CA 94720.

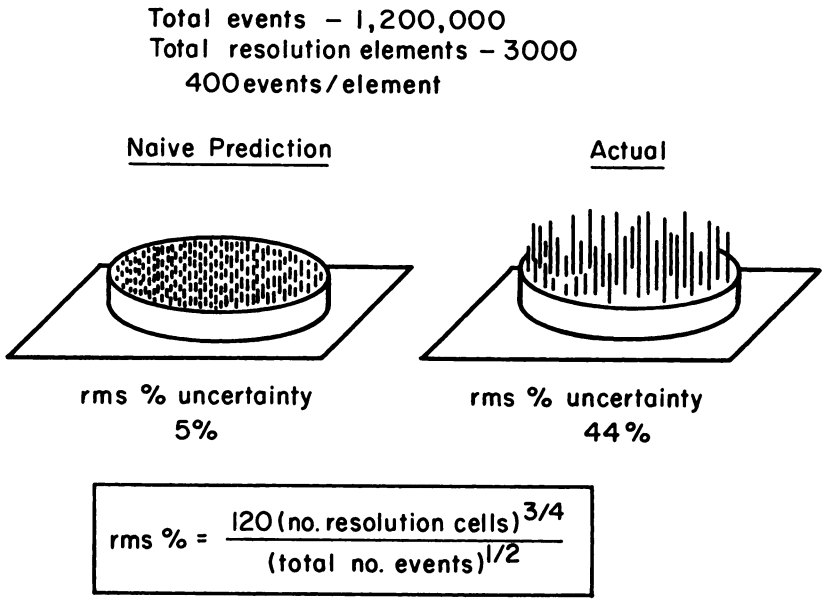

FIG. 1. Calculation of rms statistical uncertainty for uniform disc of activity.

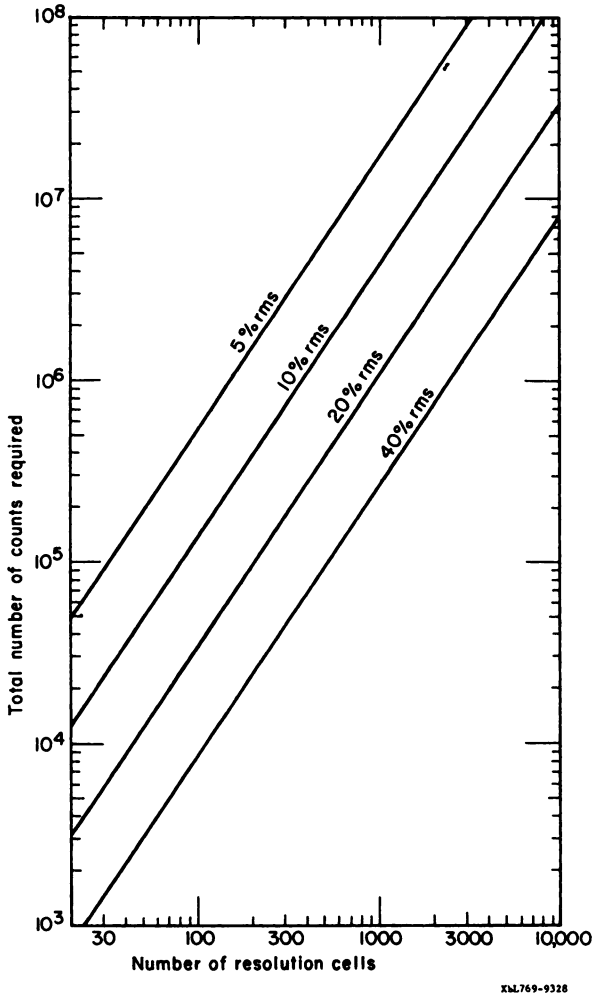

FIG. 2. Predicted statistical uncertainty as function of effective number of resolution cells and total number of detected events (Ref. 1).

total. If the resolution requirements are reduced to 300 cells, however, the required number of detected events is reduced to 190,000. It would thus appear that only very poor resolution is possible with dynamic transverse-section imaging because both positron coincidence and single gamma imaging systems have counting rates typically limited to 10,000 per second per transverse section. While the equation in Fig. 1 holds for situations for nearly uniform activity (such as xenon or krypton brain or lung imaging), it does not cover equally important cases (such as heart and kidney studies) where most of the activity lies in only 20–30% of the resolution cells. A modification to accommodate such nonuniform distributions results in a reduction of the expected errors by as much as a factor of five, which is equivalent to the injection of $\frac{1}{25}$ of the tracer dose, or a decrease in imaging time by a factor of 25. We report here the relationships between uncertainties, contrast, total number of detected events, and number of effective resolution cells for cases of one or two organ (target) areas of approximately uniform activity surrounded by a uniform background. Attenuation in tissue is not explicitly considered here; however, in a previous study (*1*), we found that for an equal number of detected events, the uncertainty is increased by about 1.3 due to errors associated with compensation for attenuation in a 20-cm diameter cylinder of water containing a uniform distribution of Tc-99m.

METHODS

The models used for simulation are illustrated in Fig. 3. Circular image arrays 64 pixels across were used with 100 projection angles and 100 bins per

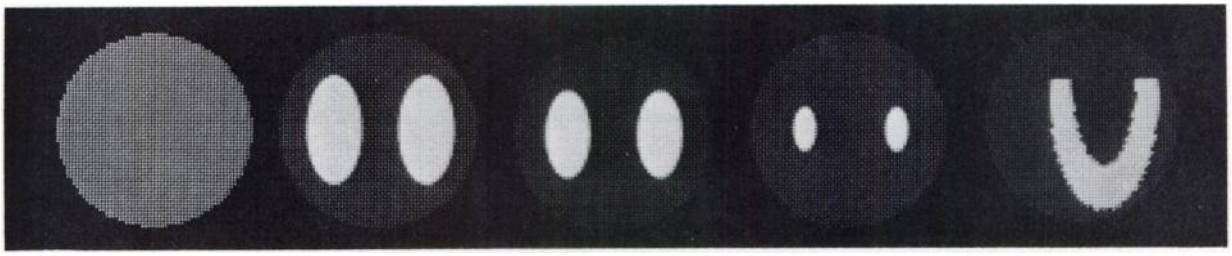

FIG. 3. Models used for simulation of statistical errors under various organ-to-background (contrast) conditions, and for various numbers of total detected events.

projection. The objects used represented kidneys and a heart "U," surrounded by a circular background region 60 pixels in diameter. Of the ~2830 pixels that contained activity, the fractions occupied by the object of interest were 30%, 20%, and 5%. Contrasts (target-to-background) assigned to each model were 4:1, 6:1, 11:1, and 31:1. A uniform disc, 60 pixels in diameter, was also used. For each of the contrast-percent-area models, four runs were made for differing detected-event totals as follows: 10^5, 5×10^5, 10^6, and 10^7. A total of 60 simulations were run using analytically generated projection data that were modified by adding Poisson noise. The majority of work was done with analytically calculated line integrals that did not involve subdividing the object into pixels. In addition, replicate studies were done by partitioning the object into rectangular pixels and then calculating projection values by integrating along rays of finite width, a practice common in computer simulations. The latter gives pseudo-data that we felt might distort the analysis. When noise is added to the pseudo-data the results are similar to those found by the correct method of forming projections. Thus quantum noise is the dominating factor in determining the signal-to-noise ratio.

The 100 projections for each reconstruction had bin sizes 0.66 that of the pixel size, in order to conform to the correct reconstruction criterion (*7*). The images were reconstructed using Goitein's iterative relaxation method (*2*) modified for conjugate gradient stepping to improve convergence. The commonly used convolution methods will give lower errors, but some reduced resolution because of their inherent smoothing. In this work we used 20 iterations, as little change was noticed between the 15th and 150th iteration provided that the pixel size was 1.5 times the projection bin size.

RESULTS AND DISCUSSION

We examined two important aspects of quantitative reliability for transverse-section imaging: (a) the fractional root-mean-square uncertainty of the regional information, and (b) the accuracy of the contrast between the target and background as measured from the reconstructed images. The rms uncertainty decreases as the fraction of the image occupied by the object decreases (Table 1). For one million events the rms uncertainty for a uniform disc of 2830 resolution cells is 52%. The uncertainty is only 15.5%, however, for an object that occupies only 20% of the resolution cells and has a target-to-background ratio of 31:1. Also, as expected, the uncertainty increases as the contrast decreases—e.g., an uncertainty of 15.5% for a 31:1 contrast increases to 24% for a 4:1 contrast if the number of detected events is one million and the object occupies 20% of the resolution cells. We found little difference between the results for the kidneys and the heart "U" when both occupied 20% of the field.

Based on the results of 60 experiments, summarized in Table 1, we derived a recipe that allows us to predict regional uncertainties in the target under various conditions of contrast and distribution of activity. The strategy is to deduce the effective number of resolution cells, M_e, for use in Fig. 2 and in a modified form of the equation in Fig. 1,

$$\text{rms\% uncertainty in } n_t = 120\,(M_e)^{3/4}(N)^{-1/2}, \quad (1)$$

where n_t is the number of events per target resolution cell and N is the total number of events measured. M_e is related both to the contrast and to the percent of the total image occupied by the object. The recipe is derived by assuming that the effective number of resolution cells, M_e, will be the number of cells in the target plus some contribution from the cells in the background. The background contribution is estimated by weighting the number of background cells by the ratio of the background concentration to the target event concentration. Thus,

$$M_e = M_t + \frac{n_b M_b}{n_t} = M_t + \frac{M_b}{C}, \quad (2)$$

or

$$M_e = \frac{n_t M_t + n_b M_b}{n_t} = \frac{N}{n_t}, \quad (3)$$

TABLE 1. RMS PERCENTAGE ERROR* IN SIMULATED PHANTOM RECONSTRUCTIONS COMPARED WITH EQ. (4) (IN PARENTHESES)

Events	5% Kidney ($M_t = 140$ $M_b = 2690$)†				20% Kidney ($M_t = 555$ $M_b = 2275$)				20% Heart "U" ($M_t = 555$ $M_b = 2275$)		30% Kidney ($M_t = 850$ $M_b = 1980$)				100% Disc $M_t = 2830$ $M_b = 0$)
	Contrast				Contrast				Contrast		Contrast				
	31:1	11:1	6:1	4:1	31:1	11:1	6:1	4:1	31:1	4:1	31:1	11:1	6:1	4:1	——
10^7	2.8 (2.2)	2.7 (3.3)	3.8 (4.5)	4.9 (5.8)	5.4 (4.8)	5.6 (5.5)	6.7 (6.4)	7.8 (7.4)	5.4 (4.8)	8.3 (7.4)	7.1 (6.3)	7.6 (6.9)	7.8 (7.6)	8.9 (8.4)	17.0 (14.7)
10^6	5.5 (7.0)	13 (10)	12 (14)	17 (18)	15.5 (15.1)	17.9 (17.4)	19.8 (20.3)	24.2 (23.3)	17.2 (15.1)	25.6 (23.3)	20.5 (19.9)	22.8 (21.8)	25.4 (24.2)	29.8 (26.7)	52.1 (46.6)
5×10^5	9.1 (9.9)	18 (15)	20 (20)	27 (26)	20.3 (21.3)	26.0 (24.6)	29.5 (28.7)	30.4 (32.9)	25.0 (21.3)	35.2 (32.9)	30.9 (28.2)	30.7 (30.9)	35.0 (34.2)	40.3 (37.7)	72.5 (65.8)
10^5	21 (22)	31 (33)	43 (45)	55 (58)	50 (48)	57 (55)	66 (64)	76 (74)	52 (48)	76 (74)	70 (63)	76 (69)	84 (76)	94 (84)	172 (147)

* With infinite statistics (no Poisson noise added) the rms errors are determined by reconstruction artifacts as follows: 5% kidney, error ~ 1%; 20% kidney, error ~ 1.6%; 30% kidney, error ~ 2%; 100% Disc, error ~ 2%.

† M_t and M_b are numbers of resolution cells in the target and background areas, respectively, for use in Eq. (4).

where n_t and n_b are the average counts per resolution cell in the target and background, respectively, $C = n_t/n_b$ is the target-to-background contrast ratio, and M_t and M_b are the numbers of resolution cells that comprise the target and background, respectively. Substitution of Eqs. (2) and (3) into Eq. (1) gives the result:

$$\text{rms \% uncertainty in } n_t = 120\left(M_t + \frac{M_b}{C}\right)^{3/4}(N)^{-1/2} \qquad (4)$$

$$= 120\,(N)^{1/4}(n_t)^{-3/4}.$$

Note that this result may be read from Fig. 2 if the effective number of resolution cells ($M_t + M_b/C$) is used as the abscissa.

The agreement between Eq. (4) and the rms errors in the reconstructed images (Table 1) is good and almost all of the differences are consistent with random uncertainties. The average value of the ratio between the observed rms errors in Table 1 and Eq. (4) values is 1.04.

Images for a 20% kidney model under three target-to-background conditions are shown for 10^7 and 10^5 collected events (Fig. 4). With low inputs, the noise becomes overwhelming and the accuracy of the reconstruction is very poor. The image quality can be improved by some simple processing, as shown in Fig. 5. Here we performed a running average with a 3 × 3 Hann filter and increased the contrast to obtain the processed image. The remarkable improvement in image quality should not mask the poor quantitative information portrayed by these data.

Uncertainty in contrast. In Table 2 we show the ability to quantitate the average target-to-background ratio for many of the examples of Table 1. All kidney pixels were used except those two to three pixels from the edge. Because of the low values and relatively large uncertainty in the background, the confidence intervals in Table 2 were analytically calculated from the distribution of the ratio of normally distributed means. Owing to the skewness of the ratio distribution this method gives a better estimate than the variance derived from simple propagation of errors. (The latter estimate is approximately the mean of the + and — deviations shown in Table 2.)

Notice that the recovered contrast is 29:1 for a simulation with 31:1 contrast and 10^6 events for an organ that occupies 20% of the resolution cells. The confidence in the measured contrast of 29:1 is +6 and —4; that is, 67% of the observations will lie between 35:1 and 25:1.

Practical applications. Two applications of Eq. (4) are of interest for potential dynamic transverse-section imaging. They relate to the following questions: (a) how much activity must be detected to image the myocardium with 1 cm FWHM and 20% uncertainty? and (b) what is the resolution we can achieve in 1-sec dynamic transverse-section images of cerebral blood flow after a 20-mCi injection of a nondiffusible tracer?

Assume that a transverse section of the heart occupies 70 resolution cells, or 10% of a total of 700; the myocardium-to-lung ratio is 4:1; and the desired uncertainty is 20% per myocardial resolution cell. For a chest 30 cm in diameter this corresponds to 1 cm × 1 cm resolution cells. Inverting Eq. (4), we find that the required number of events is

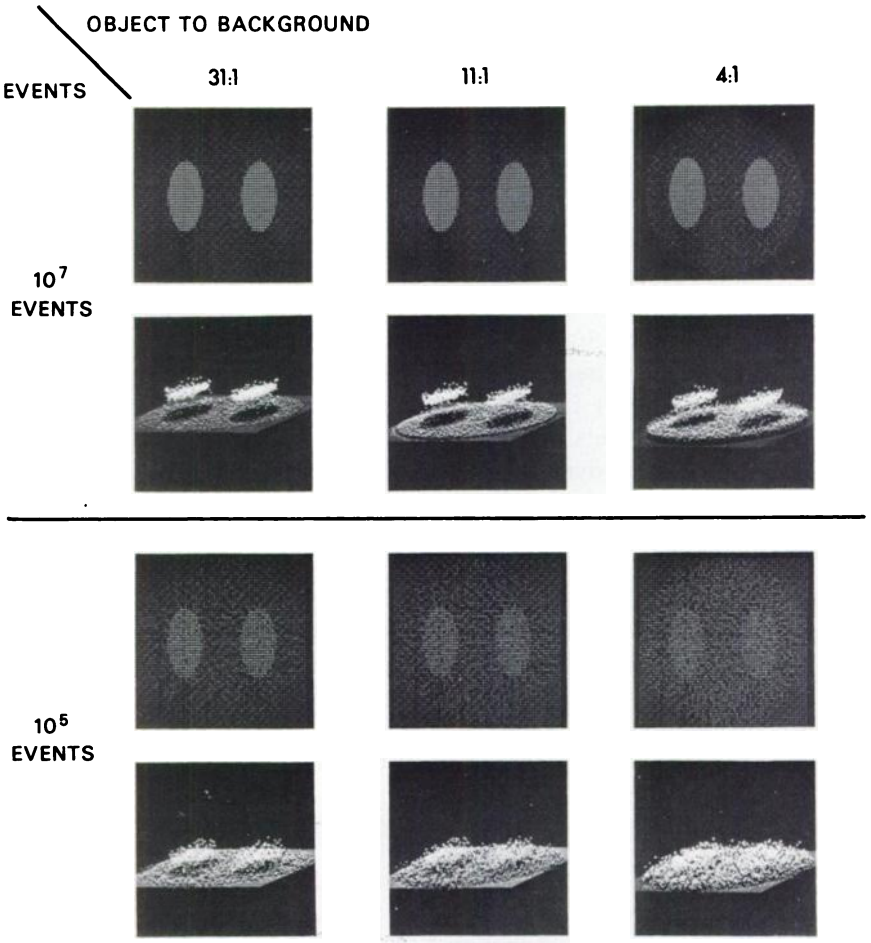

FIG. 4. Selected images illustrating results for 20% kidney model.

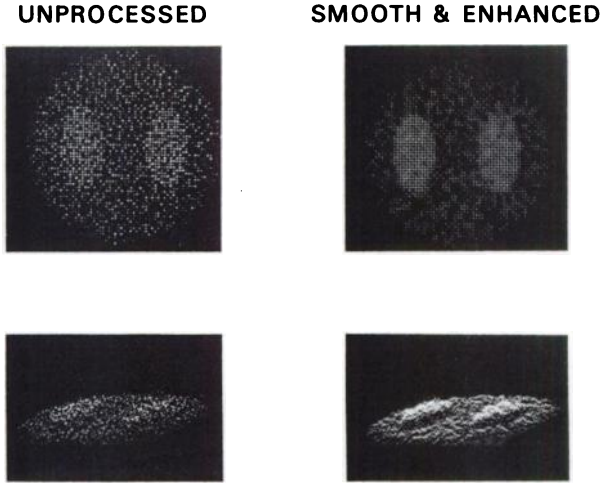

FIG. 5. Example of 10^5 events and 4:1 contrast for 20% kidney model showing image processing commonly used to give improved visual impact to statistically poor image without, however, improving reliability of data. In the unprocessed image, rms uncertainty is 76% per target pixel and processed image shows little more than the sign of reconstructed values.

$$N = \left(\frac{120}{\%\ \text{uncertainty}}\right)^2 \left(M_t + \frac{M_b}{C}\right)_{3/2}$$
$$= 36 \times \left(70 + \frac{630}{4}\right)^{3/2} \quad (5)$$
$$= 124{,}000 \text{ events.}$$

For a positron-imaging device with a sensitivity of 30 events/sec/(μCi/axial cm) and an activity of 10 mCi of Rb-82, K-38, Rb-81, or C-11 and N-13 radiopharmaceuticals, we must count for 10 min to obtain 124,000 events in each 100-msec period of the cardiac cycle for a heart rate of 60 per min. Thus, it is possible to do low-resolution myocardial metabolism and electrolyte-exchange kinetic studies. Due to the 75-sec half-life of Rb-82, multiple 10-mCi injections are required.

Another example of the application of Eqs. (4) and (5) is in determining the statistical limitations of dynamic cerebral blood-flow imaging in transverse section. Suppose we would be satisfied with a cerebral blood-flow resolution of 2 × 2 cm, or approximately 80 resolution cells for a circular reconstruction. Using an i.v. bolus injection of a nondiffusible tracer

such as Rb-82 we wish to determine the amount of activity needed for 20% rms uncertainty in 1-sec frames under the assumption that 30% of the resolution cells have four times the activity of the other resolution cells during most of the flow study. Using Eq. (5),

$$N = 36 \times \left(24 + \frac{56}{4}\right)^{3/2} = 8{,}400 \text{ events.} \quad (6)$$

If we inject 20 mCi, of which 5 mCi transit through the brain over an 8-sec period, we can assume an activity density of 300 μCi per axial cm. With an imaging system having a sensitivity of 30 events/sec/(μCi per axial cm) in a 20-cm head we have the required 9,000 events per second.

Recent work on dynamic transverse-section imaging has demonstrated the direct imaging of cerebral blood flow in 5-sec frames using the Positome (Brookhaven/Montreal 32-detector system) (*8*) that has a resolution of 3 cm FWHM. The rms uncertainties reported in that study are far more optimistic than would be concluded from the formulations in this paper. This discrepancy appears to be due to their assumption that the s.d. is the square root of the number of reconstructed events in a 1 cm × 1 cm picture element (Fig. 1, left).

CONCLUSION

The random uncertainties in quantitative information deduced from computed transverse sections of nonuniform activity distribution can be calculated from

$$\text{rms \% uncertainty in } n_t = 120\left(M_t + \frac{M_b}{C}\right)^{3/4}(N)^{-1/2} = 120(N)^{1/4}(n_t)^{-3/4}, \quad (4)$$

where N = total number of events measured, n_t is the average number of events per target resolution element, C is the target-to-background ratio, and M_t and M_b are the numbers of resolution elements that comprise the target and background areas, respectively. For uniform activity, $M_b = 0$.

Using these formulae we have shown the theoretical possibility of imaging the myocardium in transverse section with 20% uncertainty in 1 cm × 1 cm regions using 10 mCi injections of short-half-life positron emitters, and have demonstrated that quantitative dynamic transverse-section imaging of the brain will be limited to resolution elements of 2 × 2 cm after the injection of 20 mCi of nondiffusible tracer. The situation will be improved for diffusible tracers.

Previous publications dealing with error propagation in reconstruction tomography have dealt with the specific case of a uniformly distributed object. This paper approaches the more realistic conditions of a

TABLE 2. MEASURED CONTRAST

Events	5% Kidney					20% Kidney					30% Kidney				
	31:1	Contrast 11:1	6:1	4:1		31:1	Contrast 11:1	6:1	4:1		31:1	Contrast 11:1	6:1	4:1	
10^7	+2.9	+0.4	+0.2	+0.1		+2.5	+0.4	+0.1	+0.1		+3.5	+0.4	+0.1	+0.1	
	32.0	11.1	6.0	4.0		29.8	10.7	5.9	3.9		31.3	10.9	5.9	3.9	
	−2.6	−0.4	−0.2	−0.1		−2.3	−0.4	−0.1	−0.1		−3.0	−0.4	−0.1	−0.1	
10^6	+6.7	+1.1	+0.5	+0.3		+5.9	+1.0	+0.4	+0.3		+11	+1.1	+0.4	+0.2	
	33.3	9.9	5.8	4.0		29.2	11.0	5.9	4.0		33.5	10.5	6.0	4.2	
	−5.0	−0.9	−0.5	−0.3		−4.4	−0.9	−0.4	−0.2		−7.0	−1.0	−0.4	−0.2	
5×10^5	+16	+1.5	+1.3	+0.5		+14	+2.0	+0.6	+0.3		+23	+1.8	+0.6	+0.3	
	38.9	9.6	6.4	3.9		36.5	11.4	5.8	3.9		39	11.0	6.0	4.0	
	−9.2	−1.3	−1.0	−0.4		−8.3	−1.5	−0.5	−0.3		−11	−1.4	−0.5	−0.3	
10^5	+55	+6.2	+2.3	+1.5		+219	+8.5	+2.1	+1.1		+402	+8.8	+2.2	+0.9	
	41	11.6	6.1	4.1		45	13.8	6.7	4.4		42	13.6	6.8	4.3	
	−16	−3.2	−1.4	−0.9		−22	−4.0	−1.4	−0.8		−22	−4.0	−1.4	−0.7	

distribution of high-target activity in a background of lower concentration. Further refinements for various-shaped objects and relative positions of objects will lead to better prediction recipes; however, Eq. (4) should give useful estimates for most situations encountered in nuclear medicine.

ACKNOWLEDGMENTS

This work was supported by NCI Contract NIH YO1-CB-50304, NCI Grant RO1 CA-17566-01, and by the U.S. Department of Energy. We are indebted to Dr. Michael Phelps and coworkers who offered critical comments on this paper.

REFERENCES

1. BUDINGER TF, DERENZO SE, GULLBERG GT, et al: Emission computer assisted tomography with single-photon and positron annihilation photon emitters, *J Comp Assist Tomog* 1: 131–145, 1977

2. GOITEIN M: Three-dimensional density reconstruction from a series of two-dimensional projections. *Nucl Instr Meth* 101: 509–518, 1972

3. FRIEDMAN MI, BEATTIE JW, LAUGHLIN JS: Cross-sectional absorption density reconstruction for treatment planning. *Phys Med Biol* 19: 819–830, 1974

4. SHEPP LA, LOGAN BF: The Fourier reconstruction of a head section. *IEEE Trans. Nucl. Sci.* NS-21(3): 21–43, 1974

5. TANAKA E, IINUMA TA: Correction functions for optimizing the reconstructed image in transverse section scan. *Phys Med Biol* 20: 789–798, 1975

6. CHESLER DA, ARONOW S, CORRELL JE, et al: Statistical properties and simulation studies of transverse section algorithms. In *Reconstruction Tomography in Diagnostic Radiology and Nuclear Medicine*, University Park Press, 49–58, 1977

7. HUESMAN RH: The effects of a finite number of projection angles and finite lateral sampling of projections on the propagation of statistical errors in transverse section reconstruction. *Phys Med Biol* 22: 511–521, 1977

8. YAMAMOTO YL, THOMPSON CJ, MEYER E, et al: Dynamic positron emission tomography for study of cerebral hemodynamics in a cross section of the head using positron-emitting ^{68}Ga-EDTA and ^{77}Kr. *J Comput Assist Tomog* 1: 43–56, 1977